

ChinaRiceCalendar-Seasonal Crop Calendars for Early, Middle, and Late Rice in China

Hui Li¹, Xiaobo Wang^{2,*}, Shaoqiang Wang^{1,2,3,4,*}, Jinyuan Liu¹, Yuanyuan Liu², Zhenhai Liu², Shiliang Chen^{1,2}, Qinyi Wang¹, Tongtong Zhu¹, Lunche Wang¹, Lizhe Wang⁵

¹Key Laboratory of Regional Ecology and Environmental Change, School of Geography and Information Engineering, China University of Geosciences, Wuhan, 430074, China

²Key Laboratory of Ecosystem Network Observation and Modeling, Institute of Geographic Sciences and Natural Resources Research, CAS, Beijing, 100101, China

³State Key Laboratory of Biogeology and Environmental Geology, China University of Geosciences, Wuhan 430074, China;

⁴College of Resources and Environment, University of Chinese Academy of Sciences, Beijing 100049, China;

⁵Hubei Key Laboratory of Intelligent Geo-Information Processing, China University of Geosciences, Wuhan 430074, China

*Correspondence to: Xiaobo Wang (wxbwxb1995@163.com); Shaoqiang Wang (sqwang@igsnr.ac.cn)

Abstract. Long-time series and large-scale rice calendar datasets provide valuable information for agricultural planning and field management in rice-based cropping systems. However, current regional-level rice calendar datasets do not accurately distinguish between rice seasons in China, causing uncertainty in crop model simulation and climate change impact analysis. Based on satellite remote sensing data, we extracted transplanting, heading, and maturity dates of early-, middle-, and late-season rice across China from 2003 to 2022, and established a multi-season rice calendar dataset named ChinaRiceCalendar. Overall, the ChinaRiceCalendar dataset shows a good agreement with field-observed phenological dates of early, middle, and late rice in Chinese Agricultural Meteorological Stations (AMSS). According to the calendar data from 2003 to 2022, the transplanting dates for early, middle, and late rice shifted by +5.4, +2.6, and -5.7 DOY/decade, respectively; the heading date for early, middle, and late rice shifted by +5.5, -2.8, and -2.7 DOY/decade, respectively; the maturity date for early, middle, and late rice shifted by +3.2, -3.6, and -5.1 DOY/decade, respectively. The ChinaRiceCalendar can be utilized to investigate and optimize the spatio-temporal structure of rice cultivation in China under climate and land-use change.

1 Introduction

As one of the major food crops, rice feeds nearly half of the world's population (Nelson and Gumma, 2015; Fahad et al., 2019). In the context of climate change, continued warming is projected to result in shorter crop growth periods, lower rice productivity, and food insecurity in the Asian monsoon region

36 (Carleton, 2017; Zhao et al., 2017; IPCC, 2022). Revealing changes in rice phenology will facilitate
37 timely adjustment of planting time, rice cultivars, and cropping systems under global warming (Waha
38 et al., 2013; Wang et al., 2022; Wang et al., 2024). Moreover, a dynamic rice calendar with key
39 phenological dates is integral to agricultural monitoring and farmer support systems (Laborte et al.,
40 2017; Fritz et al., 2019; Mishra et al., 2021). Large-scale rice calendars can contribute to more reliable
41 simulations of crop growth and yield at regional and global scales (Franke et al., 2020).

42
43 Satellite remote sensing is an effective tool for detecting long-term trends in crop phenology at the
44 regional scale (Xiao et al., 2006; Kotsuki and Tanaka, 2015; Luo et al., 2020; Gao and Zhang, 2021;
45 Mishra et al., 2021). Crop phenology detection methods based on remote sensing vegetation indices
46 (VIs) can be categorized into threshold, inflection point, and shape model approaches. The threshold
47 approaches assume that a development stage begins when the VI value exceeds a predefined threshold
48 (Jönsson et al., 2004; Boschetti et al., 2009; Pan et al., 2015; Guo et al., 2016). The inflection point
49 approaches reconstruct the VI time-series curve by filter smoothing or function fitting, and then
50 corresponds the maxima, minima, and inflection points on the curve to the key phenological events
51 (Zhang et al., 2003; Sakamoto et al., 2005; Sun et al., 2009; Wang et al., 2019). The shape model
52 approaches fit observed VI time-series curves by geometric scaling a robust standard VI time-series
53 curve for the specific crop to identify development stages (Sakamoto et al., 2010; More et al., 2016;
54 Zeng et al., 2016; Sakamoto et al., 2018). In addition to the methods based on time series of VIs, there
55 are also rule-based algorithms that integrate multiple approaches and indicators to detect crop
56 phenology, such as the PhenoRice algorithm proposed by Boschetti et al. (2017). The PhenoRice
57 algorithm, which combines the advantages of threshold and inflection point approaches, utilizes the
58 Enhanced Vegetation Index (EVI), the Normalized Difference Flood Index (NDFI), and the land
59 surface temperature (LST) to estimate rice planting dates. The PhenoRice algorithm excels at
60 extracting rice phenology in multiple cropping systems and has been widely used in East Asia, South
61 Asia, Southeast Asia, and Europe (Busetto et al., 2019; Liu et al., 2020; Mishra et al., 2021). However,
62 the performance of the PhenoRice algorithm depends on the division of rice seasons, which requires
63 expert knowledge about rice-based cropping systems in different regions (Mishra et al., 2021).

64
65 In China, there are at least three rice-growing seasons (early, middle, and late seasons) in diverse
66 rice-based cropping systems (e.g., single-rice, double-rice, rice-wheat, rice-rapeseed, and
67 rice-vegetable systems) (Frolking et al., 2002; Qiu et al., 2003; Cao et al., 2021; He et al., 2021).
68 Generally, early, middle, and late-season rice in China are transplanted around Day Of Year (DOY)
69 80-130, DOY 130-180, and DOY 180-230, respectively. Their typical maturity dates align with DOY
70 160-220, DOY 240-290, and DOY 270-330, respectively. Although field observations are important
71 data sources for studying rice calendars in different growing seasons, they are usually limited by spatial
72 and temporal discontinuities (Zhao et al., 2016; Wang et al., 2017). Therefore, previous studies have
73 typically utilized satellite remote sensing products to establish rice calendar datasets at the regional
74 scale (Shihua et al., 2014; Liu et al., 2019; Bai and Xiao, 2020; Luo et al., 2020; Mishra et al., 2021).
75 Nevertheless, these calendar datasets based on satellite remote sensing do not rationally classify rice
76 growing seasons across China. For example, the dataset ChinaCropPhen1km only distinguishes
77 between early and late rice in double-rice systems (Luo et al., 2020); the assumptions of the dataset
78 RICA about rice heading dates in different seasons do not correspond to the realities in China (Mishra
79 et al., 2021); Shen et al. (2023) produced high-resolution distribution maps of single-season rice but did

80 not explore multiple rice cropping systems. Early-, middle- and late-season rice in China are not only
81 planted at different times, but also have distinguishing varietal characteristics, such as different
82 temperature and photoperiod sensitivities (Zong et al., 2021). Thus, a crop calendar that accurately
83 classifies rice seasons will provide reliable data for agricultural models to calibrate crop parameters at
84 the variety level. Moreover, effective identification of different rice seasons will help analyze the
85 response and adaptation of rice phenology to climate change.

86
87 Therefore, to address the shortcomings of the existing rice calendar datasets in China, we attempted to
88 improve the PhenoRice algorithm and use satellite remote sensing data to (1) establish crop calendars
89 for early, middle, and late rice in China; (2) validate the extracted rice calendars in different growing
90 seasons; and (3) explore the spatio-temporal changes of rice calendar dates in major agricultural zones
91 across China from 2003 to 2022.

92 **2 Data and Methodology**

93 **2.1 Study area**

94 We selected seven agricultural zones in China as the study area: the Northeast Plain (NP),
95 Huanghuaihai Plain (HP), Loess Plateau (LP), Middle and Lower Yangtze River Region (MLY), South
96 China Region (SC), Yunnan-Guizhou Plateau (YGP), and Sichuan Basin and Surrounding Region
97 (SCS) (Fig. 1). Due to limited hydrothermal resources, the NP and HP zones mainly cultivate
98 single-season rice. Early, middle, and late rice exist in different cropping systems in the MLY zone.
99 The SC zone has a higher cropping frequency than other zones and usually cultivates rice twice a year.
100 Parts of Hainan Province cultivate rice three times a year. Agricultural zoning data were obtained
101 from Resources and Environment Science and Data Center
102 (<https://www.resdc.cn/data.aspx?DATAID=275>).

103 **2.2 Data**

104 **2.2.1 Satellite Imagery**

105 MODIS (Moderate Resolution Imaging Spectroradiometer) remote sensing data are widely used in
106 crop phenology detection because of their excellent performance in temporal and spatial continuity
107 (Reed et al., 1994; Zhang et al., 2003; Zhao et al., 2011; Son et al., 2013). We selected two MODIS
108 EVI products for the study area during 2003–2022: MOD13Q1 (TERRA data) and MYD13Q1 (AQUA
109 data) (<https://doi.org/10.5067/MODIS/MOD13Q1.061>). Because the TERRA and AQUA data are
110 based on the synthetic period of moving eight days from each other, the time series of the two 16-day
111 products of MOD13Q1 and MYD13Q1 have a temporal resolution of 8 days (Boschetti et al., 2017).
112 The red (ρ_{RED}) and near-red (ρ_{SWIR}) bands of MOD13Q1 and MYD13Q1 were used to calculate the
113 Normalized Flooding Index (NDFI) (Eq. 1). The Pixel Reliability, Usefulness Index, and Blue Band
114 Reflectance from MOD13Q1/MYD13Q1 were used to assess data quality. The Land Surface
115 Temperature (LST) product MOD11A2 (<https://doi.org/10.5067/MODIS/MOD11A2.061>) were
116 employed to estimate land surface temperature during rice planting.

117
$$NDFI = \frac{\rho_{RED} - \rho_{SWIR}}{\rho_{RED} + \rho_{SWIR}} \quad (1)$$

118 All above raster data were downloaded and spatially aggregated to 1km resolution by the Google Earth
119 Engine (GEE) platform and the Python package of Geemap (Wu, 2020).

120 **2.2.2 Validation Data**

121 We collected field observations including transplanting, heading, and maturity dates of early, middle
122 (single-season), and late rice between 2003 and 2013 from 338 Agricultural Meteorological Stations
123 (AMSS, <https://data.cma.cn/>) in China. Moreover, we compared ChinaRiceCalendar with other
124 multi-season and regional-scale calendar datasets, including the RiceAtlas dataset based on the
125 agricultural statistics (Laborte et al., 2017), the ChinaCropPhen1km dataset based on the Global Land
126 Surface Satellite (GLASS) leaf area index (LAI) products (Luo et al., 2020), and the RICA dataset
127 based on the MOD13Q1/MYD13Q1 products (Mishra et al., 2021).

128 **2.2.3 Additional Data**

129 Cropland data were obtained from the International Geosphere-Biosphere Program (IGBP)
130 classification of the MODIS land cover product (MCD12Q1) from 2003 to 2022
131 (<https://doi.org/10.5067/MODIS/MCD12Q1.006>). Digital elevation model (DEM) data used to create a
132 terrain mask were obtained from the Shuttle Radar Topography Mission (SRTM,
133 <https://srtm.csi.cgiar.org>). Both data are resampled to a spatial resolution of 1 km.

134 **2.3 Methodology**

135 The technology roadmap of this study is shown in Fig. 2.

136 **2.3.1 Data pre-processing**

137 The data pre-processing in the study falls into three steps:

138

- 139 1. The signal of agronomic flooding was used to help identify the rice transplanting period, but
140 non-agricultural wetlands may have similar flooding signals to paddy fields (Dong and Xiao,
141 2016; Han et al., 2022). Thus, the annual cropland extent from 2003 to 2020 was used to establish
142 a cropland mask to screen the cropland pixels of the MODIS EVI data.
- 143 2. Given that too high an elevation or too great a slope is unsuitable for paddy rice cultivation
144 (Gumma et al., 2011; Dong and Xiao, 2016), only the image pixels with an elevation below 2600
145 m and a slope less than 8° were selected to extract rice calendars (Han et al., 2022).
- 146 3. To reduce the impacts of cloud contamination, we deleted the image pixels with reflectance
147 greater than 0.2 in the blue band (Xiao et al., 2006).

148 **2.3.2 Estimation of rice area and cropping calendar**

149 We combined the PhenoRice algorithm (Boschetti et al., 2017) with a growing season division method
150 (Kong et al., 2022) to extract rice pixels and cropping calendars in different growing seasons. Firstly,

151 we identified possible crop heading periods based on a weighted-smoothed EVI time-series curve in
152 each image pixel. Then we input the possible heading periods into the PhenoRice algorithm to divide
153 potential growing seasons and check if the corresponding EVI time series belongs to rice. Lastly, we
154 estimated rice planting, heading, and maturity dates and categorized them into early-, middle-, and
155 late-season calendars according to the respective transplanting and maturity times.

156 ① **Divide potential growing seasons:** The PhenoRice algorithm requires a pre-specification of rice
157 heading periods in different growing seasons to extract the corresponding VI time series. To
158 reduce the uncertainty caused by the artificial division of growing seasons, we employed the
159 *phenofit* R package developed by Kong et al. (2022) to identify possible heading periods in each
160 image pixel. 1) The weighted Whittaker method in the *phenofit* R package was employed to
161 smooth the MODIS-EVI time series (Kong et al., 2022). The Whittaker smoothing function can
162 robustly capture seasonal signals with little noise interference, and it is widely used to identify
163 crop phenology (Atzberger and Eilers, 2011; Bush et al., 2017). The curve fitting mainly relies on
164 information from good-quality points, but also extracts the limited information available from the
165 marginal- and bad-quality points. During the rough fitting to the EVI time series, we categorized
166 the data quality of the observations according to their Quality Control (QC) information
167 (SummaryQA of MOD13A1) and assigned weights of 1.0, 0.5, and 0.2 to the good-, marginal-,
168 and bad-quality VI observations, respectively. 2) Following Kong et al. (2022), the possible
169 heading date (peak point date) in each crop season was identified by the smoothed EVI time series,
170 based on the rules that only one peak value is inside a growing season and two trough values
171 define a growing season. 3) The possible heading periods (peak point dates ± 16 days) detected in
172 each image pixel were input into the PhenoRice algorithm to generate the potential growing
173 seasons.

174 ② **Check if the pixel belongs to a rice-cultivated area:** Whether the pixel belongs to a rice
175 cultivated area during the selected growing season is checked using the following procedure
176 (Boschetti et al., 2017): 1) Compare the observed maximum, and minimum EVI values with the
177 corresponding thresholds for paddy fields (EVI_{max_th} , and EVI_{min_th}) to reduce misclassification
178 problems with evergreen forests and non-vegetative areas; 2) Check for the existence of a
179 maximum inflection point on the EVI curve, which must show a consistent increasing trend
180 before the maxima and a consistent decreasing trend after the maxima. The time interval between
181 the inflection points of the minimum and maximum EVI values during the season must fall within
182 the range of rice vegetative growing periods [$v11$, $v12$]; 3) Check if the meteorological conditions
183 on the day of the minimum are favourable for rice crop establishment based on a MODIS-LST
184 value above a specified threshold (LST_{th}); 4) Detect a flood signal ($NDFI \geq minndfi$) within a time
185 window ($winfl$) centred on the minimum; 5) Check if there is a consistent increase in EVI
186 observed after the minimum; 6) Check if EVI decreases by more than $decrth\%$ of the amplitude of
187 the min-max range in a time window after the maxima ($windecr$). Only if all the above
188 requirements are satisfied, the selected growing season in the pixel is labelled as a rice season.
189 The PhenoRice parameters used in the study were calibrated by the phenological observations
190 from the AMSs in China (Table 1).

191 ③ **Estimate rice planting, heading, and maturity dates:** The rice calendar dates were estimated in
192 the detected rice pixels within the rice seasons. On the EVI time-series curve, the onset date of the

193 field growth period corresponds to the date of the minimum point closest to the retained
 194 maximum; the heading time corresponds to the date of the retained maximum point; the maturity
 195 date corresponds to the date when the EVI declined by *decrth%* of the amplitude of the min-max
 196 range. Additionally, the study categorized the detected rice calendars into early, middle, and late
 197 seasons based on their respective range of transplanting and maturity dates in each province
 198 (Table 2).

199 2.3.3 Data validation

200 Taking AMS field observations as benchmarks, we evaluated the accuracy of rice calendar dates
 201 derived from four multi-season rice calendars: ChinaRiceCalendar, ChinaCropPhen1km, RiceAtlas,
 202 and RICA. These regional rice calendars can be divided into 2 categories: raster datasets
 203 (ChinaRiceCalendar and ChinaCropPhen1km) and district-level datasets (RiceAtlas and RICA). For
 204 ChinaRiceCalendar and ChinaCropPhen1km, we sought the nearest rice pixel around each AMS site
 205 for data pairing. In instances where there was no corresponding rice pixel within a 4 km radius around
 206 an AMS site, the site was excluded from the analysis. Also, we conducted a comparison between
 207 district-level rice calendars obtained from RiceAtlas and RICA, juxtaposed with AMS data distributed
 208 within the respective districts. Two criteria were used to evaluate the accuracy of the estimated rice
 209 areas and cropping dates in each season, namely Root Mean Squared Error (RMSE, Eq. (2)) and R² (Eq.
 210 (3)):

$$211 \quad \text{RMSE} = \sqrt{\frac{1}{N} \sum_{i=1}^N (\text{true}_i - \text{est}_i)^2} \quad (2)$$

$$212 \quad R^2 = \left(\frac{\sum_{i=1}^N (\text{est}_i - \overline{\text{est}})(\text{true}_i - \overline{\text{true}})}{\sqrt{\sum_{i=1}^N (\text{est}_i - \overline{\text{est}})^2} \sqrt{\sum_{i=1}^N (\text{true}_i - \overline{\text{true}})^2}} \right)^2 \quad (3)$$

213 where true_i is the true value in the *i*th province or AMS; est_i is the corresponding estimated value;
 214 $\overline{\text{est}}$ and $\overline{\text{true}}$ denote the mean of the estimated and true values, respectively; *N* is the number of
 215 provinces or AMSs.

216

217 Additionally, in order to investigate the historical shifts of rice phenological dates in China, we
 218 analyzed the trends of rice planting, heading, and maturity dates at the county level by a
 219 Sen+Mann-Kendall trend analysis at a significance level of 0.05. The trend analysis method is detailed
 220 in Gocic et al. (2013).

221 3 Result

222 3.1 Validation of ChinaRiceCalendar

223 The key phenological dates estimated in the study show high consistency with the data from AMSs
 224 (Fig. 3). The R² between rice phenological dates from ChinaRiceCalendar and AMSs is 0.95. The R²
 225 between ChinaRiceCalendar and AMS data for transplanting, heading, and maturity dates in China is
 226 0.91, 0.88, and 0.90, respectively. The RMSEs of transplanting, heading, and maturity dates in
 227 ChinaRiceCalendar are approximately 14 days. The R² between rice phenological dates from

228 ChinaRiceCalendar and AMS data for early, middle, and late rice is 0.91, 0.94 and 0.90, respectively.

229

230 Also, we calculated the RMSE of the estimated rice cropping dates in the seven agricultural regions in
231 China (Fig. 4). Overall, the estimated rice calendars are more accurate in northern China than in the
232 south. For early-season rice, the RMSE average of the estimated cropping dates is 12.73, 12.43, and
233 14.53 days in the MLY, SC, and YGP, respectively. For middle-season rice, the range of the RMSEs in
234 the seven agricultural regions is from 4.74 days in the HP to 14.34 days in the YGP. For late-season
235 rice, the RMSE average of the estimated cropping dates is 13.90, 17.54, and 14.25 days in the MLY,
236 SC, and YGP, respectively.

237 **3.2 Comparison with other calendar datasets**

238 Using AMS field observations as benchmarks, the RMSE of rice phenological dates obtained from
239 ChinaRiceCalendar, ChinaCropPhen1km, RiceAtlas, and RICA is 13.8 days, 15.0 days, 17.9 days, and
240 22.6 days, respectively. According to the accuracy evaluation at the seasonal level (Fig. 5),
241 ChinaRiceCalendar is the only dataset where the RMSE does not exceed 15 days across three rice
242 seasons. Compared with the ChinaRiceCalendar dataset, ChinaCropPhen1km exhibits suboptimal
243 performance in early-rice seasons (RMSE=18days), RiceAtlas underperforms in middle-rice seasons
244 (RMSE=22days), and RICA falls short in both middle- and late-rice seasons (RMSE>30days). Overall,
245 ChinaRiceCalendar demonstrates superior accuracy in the estimated rice calendars compared to
246 ChinaCropPhen1km, RiceAtlas, and RICA at the annual and seasonal levels in China.

247 **3.3 Spatial distribution of rice phenological dates**

248 According to the spatial distribution of the detected rice areas during 2003-2022, early and late rice
249 were mainly grown in southern China, while middle rice was widely planted in China from south to
250 north (Figs. 6 and 7). The spatial variations of rice phenology were significant in early, middle, and late
251 seasons. In the NP, HP, and LP, middle rice was transplanted around DOY150, flowered around
252 DOY230, and matured around DOY270. In the YGP, the mean transplanting date was approximately
253 DOY100 for early rice, DOY150 for middle rice, and DOY195 for late rice; the mean heading date for
254 early, middle, and late rice was DOY170, DOY230, and DOY250, respectively; the mean maturity date
255 was approximately DOY200 for early rice, DOY260 for middle rice, and DOY290 for late rice. In the
256 MLY, the mean transplanting date was approximately DOY120 for early rice, DOY160 for middle rice,
257 and DOY200 for late rice; the mean heading date was approximately DOY190 for early rice, DOY230
258 for middle rice, and DOY250 for late rice; the mean maturity date was DOY210 for early rice,
259 DOY260 for middle rice, and DOY290 for late rice. In the SC, the mean transplanting date was
260 approximately DOY100 for early rice and DOY220 for late rice; the mean heading date was
261 approximately DOY170 for early rice and DOY270 for late rice; the mean maturity date was
262 approximately DOY200 for early rice and DOY300 for late rice. For rice in the SCS, the mean
263 transplanting, heading, and maturity dates were approximately DOY130, DOY220, and DOY250,
264 respectively.

265 **3.4 Temporal changes in rice phenological dates**

266 Based on the trend analysis of rice phenological dates from 2003 to 2022 (Fig. 8), the transplanting
267 dates for early, middle, and late rice shifted by +5.4, +2.6, and -5.7 DOY/decade, respectively; the

268 heading date for early, middle, and late rice shifted by +5.5, -2.8, and -2.7 DOY/decade, respectively;
269 the maturity date for early, middle, and late rice shifted by +3.2, -3.6, and -5.1 DOY/decade,
270 respectively. According to the trend analysis result in each rice-producing county in China between
271 2003 and 2022 (Fig. 9), 27%, 12%, and 3% of the rice-producing counties showed a significant delay
272 in transplanting dates for early, middle, and late rice, respectively; meanwhile, 5%, 6%, and 25% of the
273 counties showed a significant advancement in transplanting dates for early, middle, and late rice,
274 respectively. Moreover, 27%, 9%, and 1% of the rice-producing counties in China showed a significant
275 delay in heading dates for early, middle, and late rice, respectively; meanwhile, 1%, 7%, and 22% of
276 the counties showed a significant advancement in heading dates for early, middle, and late rice,
277 respectively. Also, 24%, 6%, and 2% of the rice-producing counties in China showed a significant
278 delay in maturity dates for early, middle, and late rice, respectively; meanwhile, 2%, 14%, and 19% of
279 the counties showed a significant advancement in heading dates for early, middle, and late rice,
280 respectively. Overall, the growing season of early rice tended to be delayed, while the growing season
281 of late rice tended to advance between 2003 and 2020 in China. Additionally, the shifts in the
282 phenological dates of middle rice during 2003-2020 depended on the agricultural region (Fig. 9).

283 **4 Uncertainties in ChinaRiceCalendar**

284 This study used MODIS remote sensing data to extract rice phenological dates in various growing
285 seasons in China. The MODIS remote sensing products have an appropriate temporal resolution, long
286 time series, and good time consistency for analyzing changes in rice calendars at the regional scale.
287 Moreover, the MODIS data are easy to obtain and process on the GEE platform, allowing for
288 automated and timely updating of the calendar dataset. Nevertheless, discerning early- and late-rice
289 pixels is more difficult than identifying middle-rice pixels in MODIS data, resulting in lower accuracy
290 of the detected rice calendars in southern China (MLY, SC, SCS, YGP) than in northern China (NP,
291 HP, LP).

292
293 There are several factors leading to the incomplete identification of rice pixels in early and late seasons
294 in southern China. Firstly, the pixel-based detection of rice areas may be interfered with by the
295 contamination of clouds, aerosols, and water vapor, especially during the monsoon season when late
296 rice is transplanted (Xiao et al., 2005; Xiao et al., 2014; Clauss et al., 2016; Mishra et al., 2021).
297 Because synthetic aperture radar (SAR) can penetrate through clouds, subsequent studies could
298 combine optical and SAR images to avoid the impacts of clouds (Shen et al., 2023a). Utilizing
299 geostationary satellite observations to increase the temporal frequency of remote sensing data may also
300 be an effective way to improve accuracy of rice calendars (Shen et al., 2023b). Secondly, diverse
301 multi-cropping systems, complex topography, and the fragmentation of croplands in southern China
302 make the pixel detection for early and late rice more challenging (Dong and Xiao, 2016). Producing
303 satellite remote sensing data with higher spatial resolution and integrating multiple data sources from
304 satellite-airborne-ground observations will facilitate real-time monitoring of rice cropping areas at the
305 regional scale (Zheng et al., 2022; Sun et al., 2023). Additionally, the PhenoRice algorithm faces
306 challenges in detecting rice pixels in rainfed or upland rice systems due to the absence of clear
307 agronomic flooding signals. In China, rice is mainly planted in flooded paddy fields (Luo et al., 2022),
308 which mitigates the problems of detecting rainfed or upland rice. Last but not least, precisely
309 corresponding the image pixels from the MODIS dataset to the Agricultural Meteorological Stations

310 remains a challenge during data validation. In the future, it would be beneficial to conduct a
311 quantitative assessment to determine the representativeness of the MODIS pixels surrounding the AMS
312 site.

313

314 In this study, we improved the method of growing season division in the PhenoRice algorithm. We also
315 attempted to remove non-paddy pixels and reduce the impacts of low-quality data on the reconstruction
316 of EVI time-series curves. Although the local tuning of the PhenoRice algorithm parameters could
317 further improve the results, we employed a single configuration of EVI threshold values across China
318 because automated methods that perform robustly are essential for developing timely information about
319 crop calendars over large extents (Mishra et al., 2021). Subsequently, we will try to automate the
320 generation and updating of ChinaRiceCalendar based on the ‘rgee’ package (Aybar et al., 2023).

321 **5 Data Availability**

322 ChinaRiceCalendar is a raster dataset with 1km spatial resolution. The spatial reference system of the
323 dataset is WGS_1984_UTM_Zone_49N. The dataset currently covers 2003~2022. ChinaRiceCalendar
324 is available at <https://doi.org/10.7910/DVN/EUP8EY> (Hui Li, 2023).

325 **6 Conclusions**

326 Utilizing MODIS time series data, we established a multi-season rice calendar dataset named
327 ChinaRiceCalendar, encompassing transplanting, heading, and maturity dates of early, middle, and late
328 rice in China from 2003 to 2022. The rice phenological dates within ChinaRiceCalendar, estimated
329 through the enhanced PhenoRice algorithm, exhibit strong alignment with field observations collected
330 by Agricultural Meteorological Stations across China. The R^2 values between ChinaRiceCalendar and
331 field data for early, middle, and late rice consistently surpass 0.90, with RMSE values below 15 days in
332 three rice seasons. According to the calendar data from 2003 to 2022, the transplanting dates for early,
333 middle, and late rice shifted by +5.4, +2.6, and -5.7 DOY/decade, respectively; the heading date for
334 early, middle, and late rice shifted by +5.5, -2.8, and -2.7 DOY/decade, respectively; the maturity date
335 for early, middle, and late rice shifted by +3.2, -3.6, and -5.1 DOY/decade, respectively. In summary,
336 ChinaRiceCalendar stands as a reliable dataset for investigating and optimizing the spatio-temporal
337 dynamics of rice cultivation in China, particularly in the context of climate and land-use changes.

338 **Author Contributions:** Conceptualization and methodological, HL and XW; algorithmic
339 improvements, HL; data download and processing, JL, YL and ZL; validation, JL, SC and QW; formal
340 analysis, HL, XW, and TZ; writing-original draft preparation, HL and XW; writing-review and editing,
341 XW, SW and LW. All authors have read and agreed to the published version of the manuscript.

342

343 **Financial support:** This research has been supported by the National Natural Science Foundation of
344 China (Project Nos. 31861143015 and 32301393).

345

346 **Acknowledgments:** We would like to thank Dongdong Kong from China University of Geosciences
347 (Wuhan) for providing the R package *Phnofit* and thank Mirco Boschetti from the Italian National

348 Research Council for providing the source code of *PhenoRice*.

349

350 **Conflicts of Interest:** The authors declare no conflict of interest.

351 **References**

352 Atzberger, C. and Eilers, P.H.: Evaluating the effectiveness of smoothing algorithms in the absence of
353 ground reference measurements. *International Journal of Remote Sensing*, 32(13), 3689-3709, 2011.

354 Aybar, C. rgee: R Bindings for Calling the 'Earth Engine' API (Version 1.1.7).
355 <https://github.com/r-spatial/rgee/issues/>, 2023.

356 Bai, H. and Xiao, D.: Spatiotemporal changes of rice phenology in China during 1981 – 2010.
357 *Theoretical and Applied Climatology*, 140, 1483-1494, 2020.

358 Boschetti, M., Busetto, L., Manfron, G., Laborte, A., Asilo, S., Pazhanivelan, S. and Nelson, A.:
359 PhenoRice: A method for automatic extraction of spatio-temporal information on rice crops using
360 satellite data time series. *Remote sensing of environment*, 194, 347-365, 2017.

361 Boschetti, M., Stroppiana, D., Brivio, P. and Bocchi, S.: Multi-year monitoring of rice crop phenology
362 through time series analysis of MODIS images. *International journal of remote sensing*, 30(18),
363 4643-4662, 2009.

364 Busetto, L., Zwart, S.J. and Boschetti, M.: Analysing spatial – temporal changes in rice cultivation
365 practices in the Senegal River Valley using MODIS time-series and the PhenoRice algorithm.
366 *International Journal of Applied Earth Observation and Geoinformation*, 75, 15-28, 2019.

367 Bush, E.R., Abernethy, K.A., Jeffery, K., Tutin, C., White, L., Dimoto, E., Dikangadissi, J.T., Jump,
368 A.S. and Bunnefeld, N.: Fourier analysis to detect phenological cycles using long - term tropical field
369 data and simulations. *Methods in Ecology and Evolution*, 8(5), 530-540, 2017.

370 Cao, J., Cai, X., Tan, J., Cui, Y., Xie, H., Liu, F., Yang, L. and Luo, Y.: Mapping paddy rice using
371 Landsat time series data in the Ganfu Plain irrigation system, Southern China, from 1988 – 2017.
372 *International Journal of Remote Sensing*, 42(4), 1556-1576, 2021.

373 Carleton, T.A.: Crop-damaging temperatures increase suicide rates in India. *Proceedings of the*
374 *National Academy of Sciences*, 114(33), 8746-8751, 2017.

375 Clauss, K., Yan, H. and Kuenzer, C.: Mapping paddy rice in China in 2002, 2005, 2010 and 2014 with
376 MODIS time series. *Remote Sensing*, 8(5), 434, 2016.

377 Dong, J. and Xiao, X.: Evolution of regional to global paddy rice mapping methods: A review. *ISPRS*
378 *Journal of Photogrammetry and Remote Sensing*, 119, 214-227, 2016.

379 Fahad, S., Adnan, M., Noor, M., Arif, M., Alam, M., Khan, I.A., Ullah, H., Wahid, F., Mian, I.A. and
380 Jamal, Y.: Major constraints for global rice production, *Advances in rice research for abiotic stress*
381 *tolerance*. Elsevier, pp. 1-22, 2019.

382 Franke, J.A., Müller, C., Elliott, J., Ruane, A.C., Jägermeyr, J., Snyder, A., Dury, M., Falloon, P.D.,
383 Folberth, C. and François, L.: The GGCM Phase 2 emulators: global gridded crop model responses to

384 changes in CO₂, temperature, water, and nitrogen (version 1.0). Geoscientific Model Development,
385 13(9), 3995-4018, 2020.

386 Fritz, S., See, L., Bayas, J.C.L., Waldner, F., Jacques, D., Becker-Reshef, I., Whitcraft, A., Baruth, B.,
387 Bonifacio, R. and Crutchfield, J.: A comparison of global agricultural monitoring systems and current
388 gaps. *Agricultural systems*, 168, 258-272, 2019.

389 Frohling, S., Qiu, J., Boles, S., Xiao, X., Liu, J., Zhuang, Y., Li, C. and Qin, X.: Combining remote
390 sensing and ground census data to develop new maps of the distribution of rice agriculture in China.
391 *Global Biogeochemical Cycles*, 16(4), 38-1-38-10, 2002.

392 Gao, F. and Zhang, X.: Mapping crop phenology in near real-time using satellite remote sensing:
393 Challenges and opportunities. *Journal of Remote Sensing*, 2021, 2021.

394 Gocic, M. and Trajkovic, S.: Analysis of changes in meteorological variables using Mann-Kendall and
395 Sen's slope estimator statistical tests in Serbia. *Global and Planetary Change*, 100, 172-182, 2013.

396 Gumma, M.K., Nelson, A., Thenkabail, P.S. and Singh, A.N.: Mapping rice areas of South Asia using
397 MODIS multitemporal data. *Journal of applied remote sensing*, 5(1), 053547, 2011.

398 Guo, L., An, N. and Wang, K.: Reconciling the discrepancy in ground- and satellite-observed trends in
399 the spring phenology of winter wheat in China from 1993 to 2008. *Journal of Geophysical Research:
400 Atmospheres*, 121(3), 1027-1042, 2016.

401 Han, J., Zhang, Z., Luo, Y., Cao, J., Zhang, L., Zhuang, H., Cheng, F., Zhang, J. and Tao, F.: Annual
402 paddy rice planting area and cropping intensity datasets and their dynamics in the Asian monsoon
403 region from 2000 to 2020. *Agricultural Systems*, 200, 103437, 2022.

404 He, Y., Dong, J., Liao, X., Sun, L., Wang, Z., You, N., Li, Z. and Fu, P.: Examining rice distribution and
405 cropping intensity in a mixed single- and double-cropping region in South China using all available
406 Sentinel 1/2 images. *International Journal of Applied Earth Observation and Geoinformation*, 101,
407 102351, 2021.

408 Hui Li, Xiaobo Wang, Shaoqiang Wang, Yuanyuan Liu, Zhenhai Liu, Shiliang Chen, Qinyi Wang,
409 Tongtong Zhu, Lunche Wang, Lizhe Wang. *ChinaRiceCalendar*. Harvard Dataverse,
410 doi/10.7910/DVN/EUP8EY, 2023.

411 IPCC. *Climate change 2022: impacts, adaptation and vulnerability*.
412 <https://www.ipcc.ch/report/sixth-assessment-report-working-group-ii/>, 2022.

413 Kim, D.-H., Jang, T., Hwang, S., and Jeong, H.: Paddy rice adaptation strategies to climate change:
414 Transplanting date shift and BMP applications, *Agricultural Water Management*, 252, 106926, 2021.

415 Kong, D., McVicar, T.R., Xiao, M., Zhang, Y., Peña - Arancibia, J.L., Filippa, G., Xie, Y. and Gu, X.:
416 phenofit: An R package for extracting vegetation phenology from time series remote sensing. *Methods
417 in Ecology and Evolution*, 2022.

418 Kotsuki, S. and Tanaka, K.: SACRA – a method for the estimation of global high-resolution crop
419 calendars from a satellite-sensed NDVI. *Hydrology and Earth System Sciences*, 19(11), 4441-4461,
420 2015.

421 Laborte, A.G., Gutierrez, M.A., Balanza, J.G., Saito, K., Zwart, S.J., Boschetti, M., Murty, M., Villano,
422 L., Aunario, J.K. and Reinke, R.: RiceAtlas, a spatial database of global rice calendars and production.
423 *Scientific data*, 4(1), 1-10, 2017.

424 Liu, L., Huang, J., Xiong, Q., Zhang, H., Song, P., Huang, Y., Dou, Y. and Wang, X.: Optimal MODIS
425 data processing for accurate multi-year paddy rice area mapping in China. *GIScience & Remote*
426 *Sensing*, 57(5), 687-703, 2020.

427 Liu, Y., Zhou, W. and Ge, Q.: Spatiotemporal changes of rice phenology in China under climate change
428 from 1981 to 2010. *Climatic Change*, 157, 261-277, 2019.

429 Luo, W., Chen, M., Kang, Y., Li, W., Li, D., Cui, Y., Khan, S. and Luo, Y.: Analysis of crop water
430 requirements and irrigation demands for rice: Implications for increasing effective rainfall. *Agricultural*
431 *Water Management*, 260, 107285, 2022.

432 Luo, Y., Zhang, Z., Chen, Y., Li, Z. and Tao, F.: ChinaCropPhen1km: a high-resolution crop
433 phenological dataset for three staple crops in China during 2000–2015 based on leaf area index (LAI)
434 products. *Earth System Science Data*, 12(1), 197-214, 2020.

435 Mishra, B., Busetto, L., Boschetti, M., Laborte, A. and Nelson, A.: RICA: A rice crop calendar for Asia
436 based on MODIS multi year data. *International Journal of Applied Earth Observation and*
437 *Geoinformation*, 103, 102471, 2021.

438 More, R.S., Manjunath, K., Jain, N.K., Panigrahy, S. and Parihar, J.S.: Derivation of rice crop calendar
439 and evaluation of crop phenometrics and latitudinal relationship for major south and south-east Asian
440 countries: A remote sensing approach. *Computers and Electronics in Agriculture*, 127, 336-350, 2016.

441 Nelson, A. and Gumma, M.: A map of lowland rice extent in the major rice growing countries of Asia.
442 IRRI, Los Banos, Philippines, 2015.

443 Pan, Z., Huang, J., Zhou, Q., Wang, L., Cheng, Y., Zhang, H., Blackburn, G.A., Yan, J. and Liu, J.:
444 Mapping crop phenology using NDVI time-series derived from HJ-1 A/B data. *International Journal of*
445 *Applied Earth Observation and Geoinformation*, 34, 188-197, 2015.

446 Parmesan, C., Morecroft, M.D. and Trisurat, Y.: *Climate change 2022: Impacts, adaptation and*
447 *vulnerability*, GIEC, 2022.

448 Qiu, J., Tang, H., Froking, S., Boles, S., Li, C., Xiao, X., Liu, J., Zhuang, Y. and Qin, X.: Mapping
449 single-, double-, and triple-crop agriculture in China at 0.5° × 0.5° by combining county-scale census
450 data with a remote sensing-derived land cover map. *Geocarto International*, 18(2), 3-13, 2003.

451 Reed, B.C., Brown, J.F., VanderZee, D., Loveland, T.R., Merchant, J.W. and Ohlen, D.O.: Measuring
452 phenological variability from satellite imagery. *Journal of vegetation science*, 5(5), 703-714, 1994.

453 Sakamoto, T., Wardlow, B.D., Gitelson, A.A., Verma, S.B., Suyker, A.E. and Arkebauer, T.J.: A
454 two-step filtering approach for detecting maize and soybean phenology with time-series MODIS data.
455 *Remote Sensing of Environment*, 114(10), 2146-2159, 2010.

456 Sakamoto, T., Yokozawa, M., Toritani, H., Shibayama, M., Ishitsuka, N. and Ohno, H.: A crop
457 phenology detection method using time-series MODIS data. *Remote sensing of environment*, 96(3-4),
458 366-374, 2005.

459 Sakamoto, T.: Refined shape model fitting methods for detecting various types of phenological
460 information on major US crops. *ISPRS Journal of Photogrammetry and Remote Sensing*, 138, 176-192,
461 2018.

462 Shen, R., Pan, B., Peng, Q., Dong, J., Chen, X., Zhang, X., Ye, T., Huang, J. and Yuan, W.:
463 High-resolution distribution maps of single-season rice in China from 2017 to 2022. *Earth System
464 Science Data Discussions*, 1-27, 2023a.

465 Shen, Y., Zhang, X., Yang, Z., Ye, Y., Wang, J., Gao, S., Liu, Y., Wang, W., Tran, K.H. and Ju, J.:
466 Developing an operational algorithm for near-real-time monitoring of crop progress at field scales by
467 fusing harmonized Landsat and Sentinel-2 time series with geostationary satellite observations. *Remote
468 Sensing of Environment*, 296, 113729, 2023b.

469 Shihua, L., Jingtao, X., Ping, N., Jing, Z., Hongshu, W. and Jingxian, W.: Monitoring paddy rice
470 phenology using time series MODIS data over Jiangxi Province, China. *International Journal of
471 Agricultural and Biological Engineering*, 7(6), 28-36, 2014.

472 Son, N.-T., Chen, C.-F., Chen, C.-R., Duc, H.-N. and Chang, L.-Y.: A phenology-based classification of
473 time-series MODIS data for rice crop monitoring in Mekong Delta, Vietnam. *Remote Sensing*, 6(1),
474 135-156, 2013.

475 Sun, C., Zhang, H., Xu, L., Ge, J., Jiang, J., Zuo, L. and Wang, C.: Twenty-meter annual paddy rice
476 area map for mainland Southeast Asia using Sentinel-1 synthetic-aperture-radar data. *Earth System
477 Science Data*, 15(4), 1501-1520, 2023.

478 Sun, H., Huang, J. and Peng, D.: Detecting major growth stages of paddy rice using MODIS data. *J.
479 Remote Sens*, 13, 1122-1137, 2009.

480 Waha, K., Müller, C. and Rolinski, S.: Separate and combined effects of temperature and precipitation
481 change on maize yields in sub-Saharan Africa for mid-to late-21st century. *Global and Planetary
482 Change*, 106, 1-12, 2013.

483 Wang, J., Yu, K., Tian, M. and Wang, Z.: Estimation of rice key phenology date using Chinese HJ-1
484 vegetation index time-series images, 2019 8th International Conference on Agro-Geoinformatics
485 (Agro-Geoinformatics). IEEE, pp. 1-4, 2019.

486 Wang, X., Ciais, P., Li, L., Ruget, F., Vuichard, N., Viovy, N., Zhou, F., Chang, J., Wu, X. and Zhao, H.:
487 Management outweighs climate change on affecting length of rice growing period for early rice and
488 single rice in China during 1991–2012. *Agricultural and Forest Meteorology*, 233, 1-11, 2017.

489 Wang, X., Folberth, C., Skalsky, R., Wang, S., Chen, B., Liu, Y., Chen, J. and Balkovic, J.: Crop
490 calendar optimization for climate change adaptation in rice-based multiple cropping systems of India
491 and Bangladesh. *Agricultural and Forest Meteorology*, 315, 108830, 2022.

492 Wang, X., Wang, S., Folberth, C., Skalsky, R., Li, H., Liu, Y. and Balkovic, J.: Limiting global
493 warming to 2° C benefits building climate resilience in rice-wheat systems in India through crop
494 calendar management. *Agricultural Systems*, 213, 103806, 2024.

495 Wu, Q.: geemap: A Python package for interactive mapping with Google Earth Engine. *Journal of
496 Open Source Software*, 5(51), 2305, 2020.

497 Xiao, X., Boles, S., Frolking, S., Li, C., Babu, J.Y., Salas, W. and Moore III, B.: Mapping paddy rice
498 agriculture in South and Southeast Asia using multi-temporal MODIS images. *Remote sensing of*
499 *Environment*, 100(1), 95-113, 2006.

500 Xiao, X., Boles, S., Liu, J., Zhuang, D., Frolking, S., Li, C., Salas, W. and Moore III, B.: Mapping
501 paddy rice agriculture in southern China using multi-temporal MODIS images. *Remote sensing of*
502 *environment*, 95(4), 480-492, 2005.

503 Zeng, L., Wardlow, B.D., Wang, R., Shan, J., Tadesse, T., Hayes, M.J. and Li, D.: A hybrid approach for
504 detecting corn and soybean phenology with time-series MODIS data. *Remote Sensing of Environment*,
505 181, 237-250, 2016.

506 Zhang, X., Friedl, M.A., Schaaf, C.B., Strahler, A.H., Hodges, J.C., Gao, F., Reed, B.C. and Huete, A.:
507 Monitoring vegetation phenology using MODIS. *Remote sensing of environment*, 84(3), 471-475,
508 2003.

509 Zhang, Z., Song, X., Tao, F., Zhang, S. and Shi, W.: Climate trends and crop production in China at
510 county scale, 1980 to 2008. *Theoretical and Applied Climatology*, 123(1), 291-302, 2016.

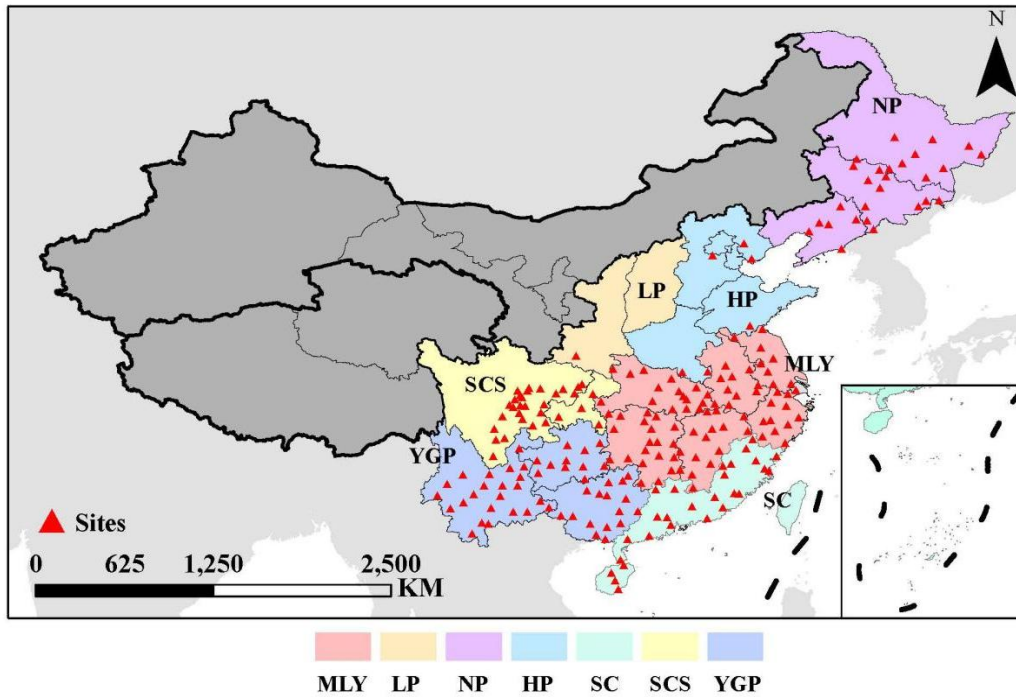
511 Zhao, C., Liu, B., Piao, S., Wang, X., Lobell, D.B., Huang, Y., Huang, M., Yao, Y., Bassu, S. and Ciaia,
512 P.: Temperature increase reduces global yields of major crops in four independent estimates.
513 *Proceedings of the National Academy of sciences*, 114(35), 9326-9331, 2017.

514 Zhao, H., Yang, Z., Di, L. and Pei, Z.: Evaluation of temporal resolution effect in remote sensing based
515 crop phenology detection studies, *International Conference on Computer and Computing Technologies*
516 *in Agriculture*. Springer, pp. 135-150, 2011.

517 Zheng, J., Song, X., Yang, G., Du, X., Mei, X. and Yang, X.: Remote sensing monitoring of rice and
518 wheat canopy nitrogen: A review. *Remote Sensing*, 14(22), 5712, 2022.

519 Zong, W., Ren, D., Huang, M., Sun, K., Feng, J., Zhao, J., Xiao, D., Xie, W., Liu, S. and Zhang,
520 H.: Strong photoperiod sensitivity is controlled by cooperation and competition among Hd1, Ghd7
521 and DTH8 in rice heading. *New Phytologist*, 229(3), 1635-1649, 2021.

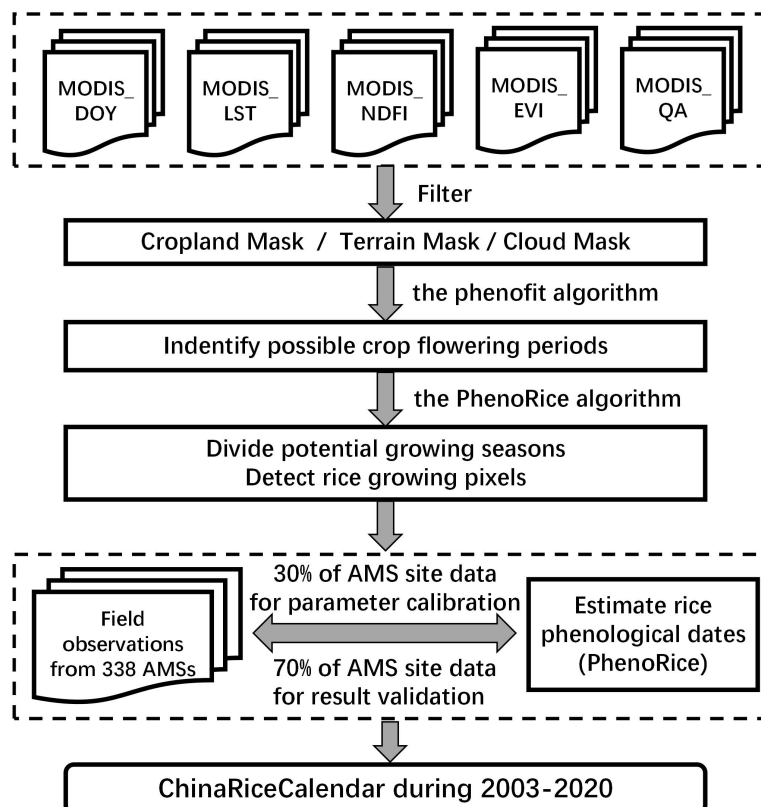
522



523

524

Fig. 1 Study area and distribution of Agricultural Meteorological Stations (AMSs) in China

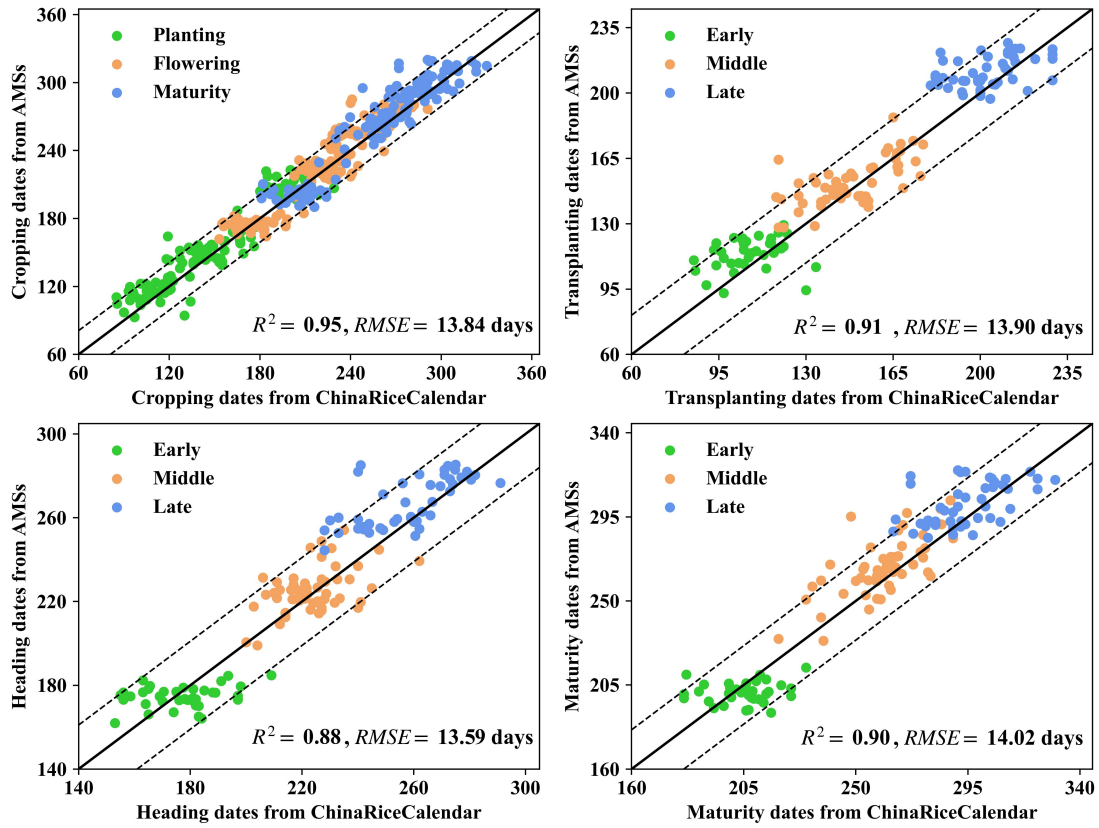


525

526

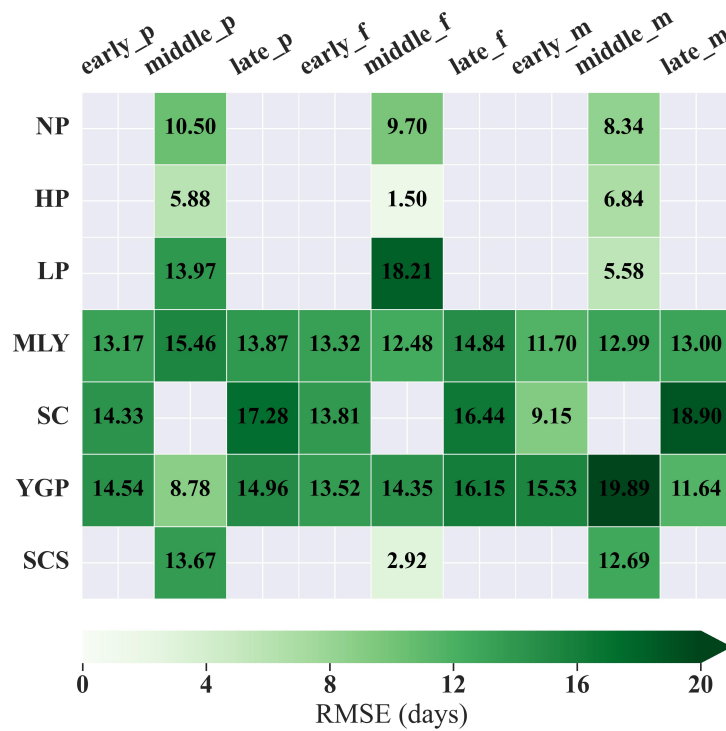
527

Fig. 2 Technology roadmap for this study



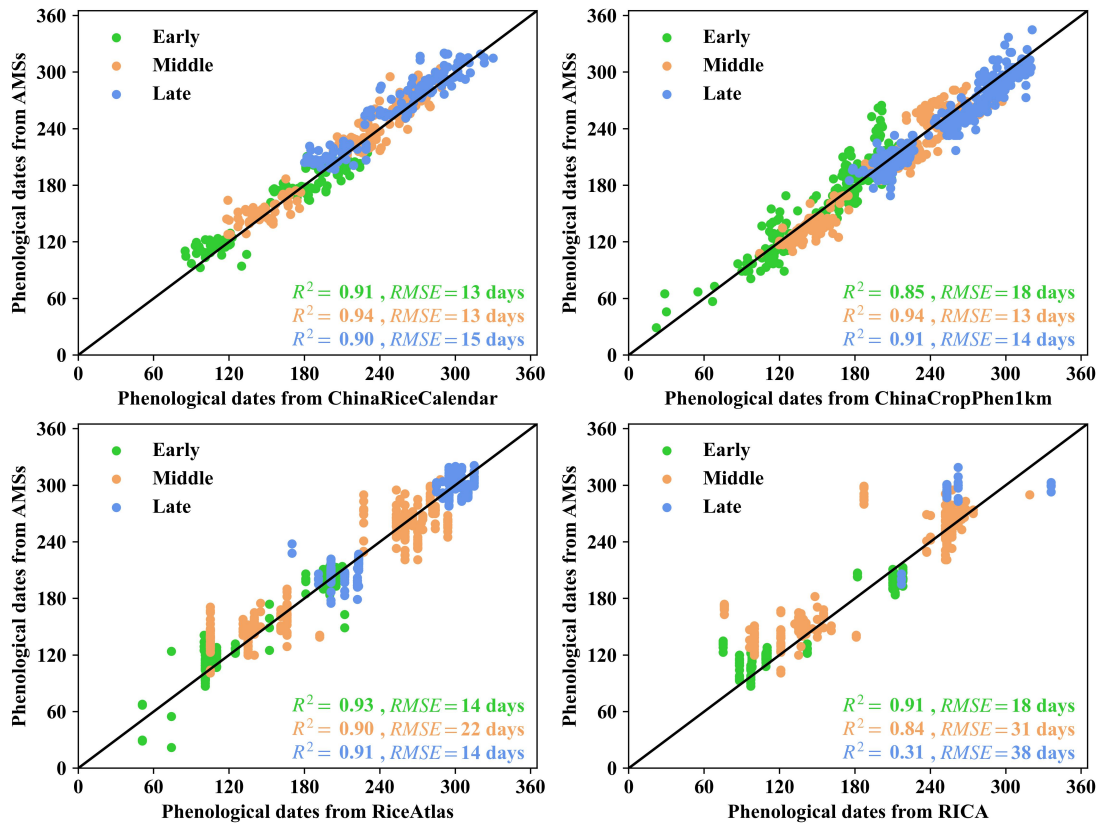
528

529 **Fig. 3 Comparison of rice phenological dates between ChinaRiceCalendar and AMS data at the**
 530 **site scale (dashed lines are ± 21 days)**



531

532 **Fig. 4 RMSEs of rice phenological dates between ChinaRiceCalendar and AMS data in main**
 533 **agricultural regions**

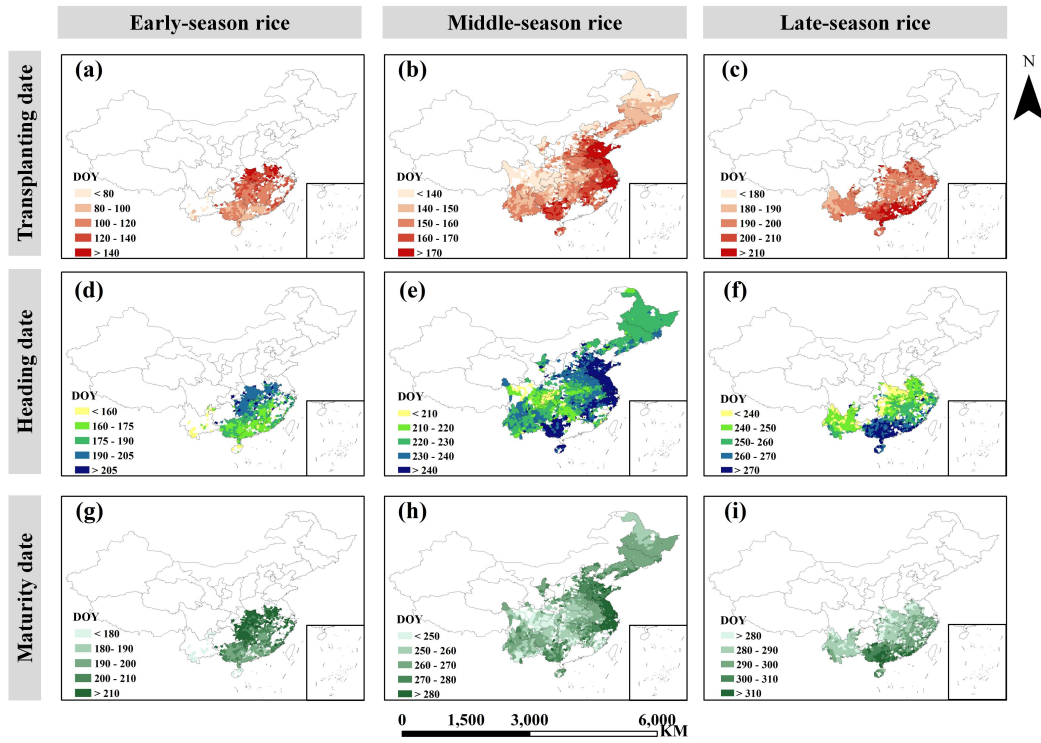


534

535 **Fig. 5 Comparison of rice phenological dates between calendar datasets and AMS data at the**
 536 **site scale in early (green), middle (orange), and late (blue) seasons.**

537

538



539

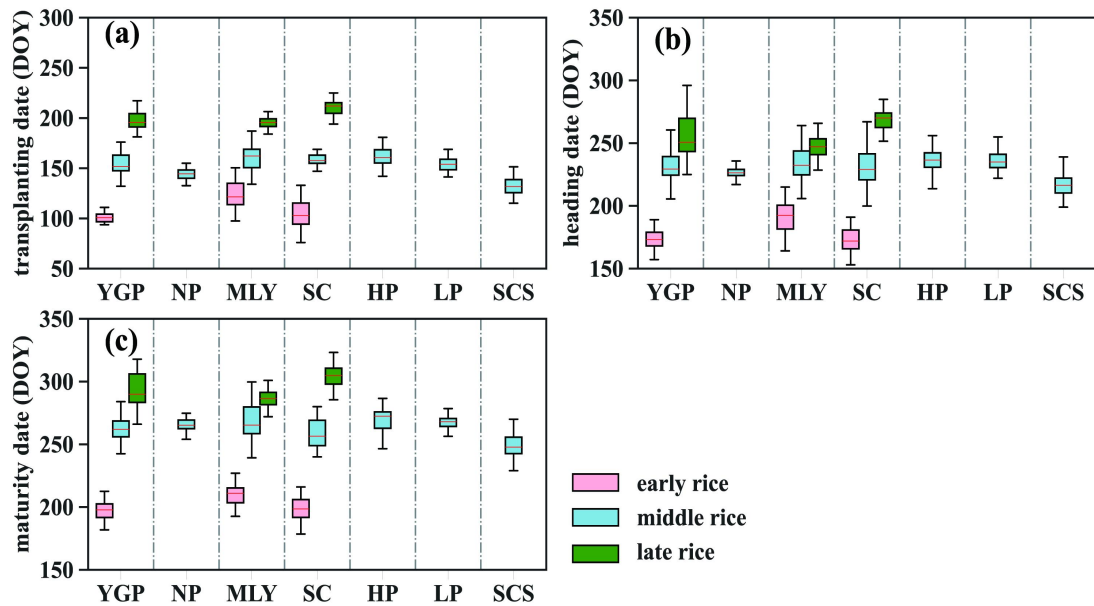
540

Fig. 6 Rice phenological dates at the county scale between 2003 and 2022 (a: early-rice transplanting dates; b: middle-rice transplanting dates; c: late-rice transplanting dates; d: early-rice heading dates; e: middle-rice heading dates; f: late-rice heading dates; g: early-rice maturity dates; h: middle-rice maturity dates; i: late-rice maturity dates)

541

542

543

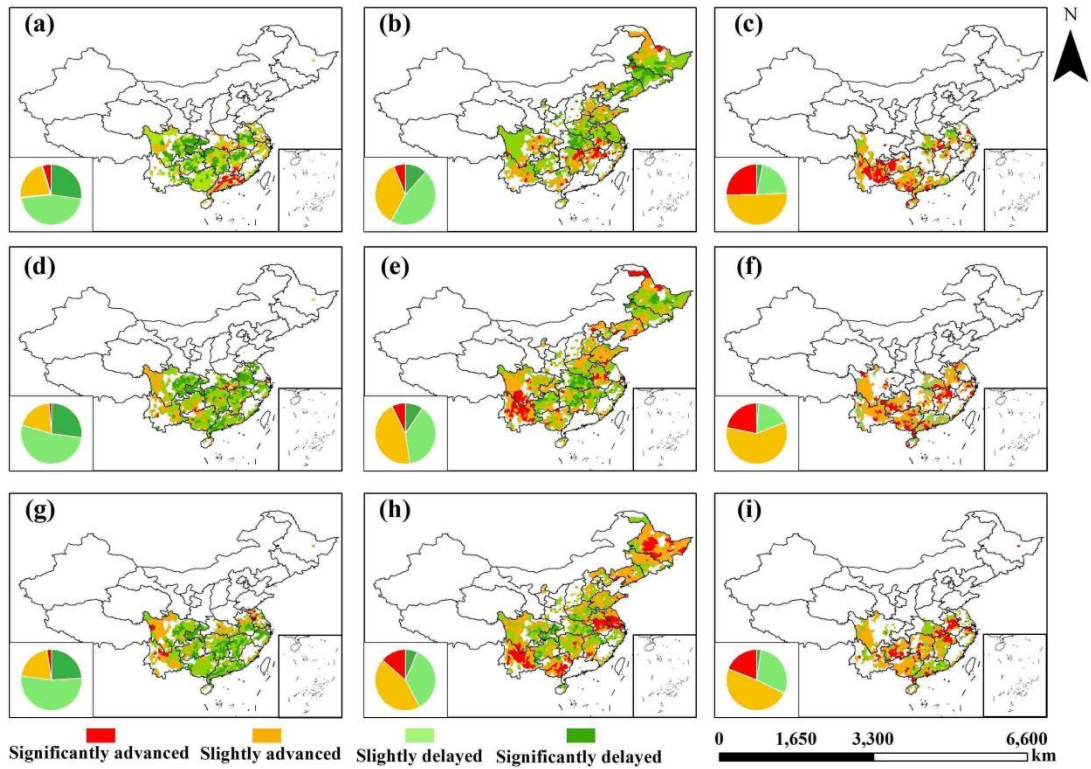


544

545

Fig. 7 Rice phenological dates in main agricultural regions between 2003 and 2022 (a: Transplanting dates; b: Heading dates; c: Maturity dates)

546



547

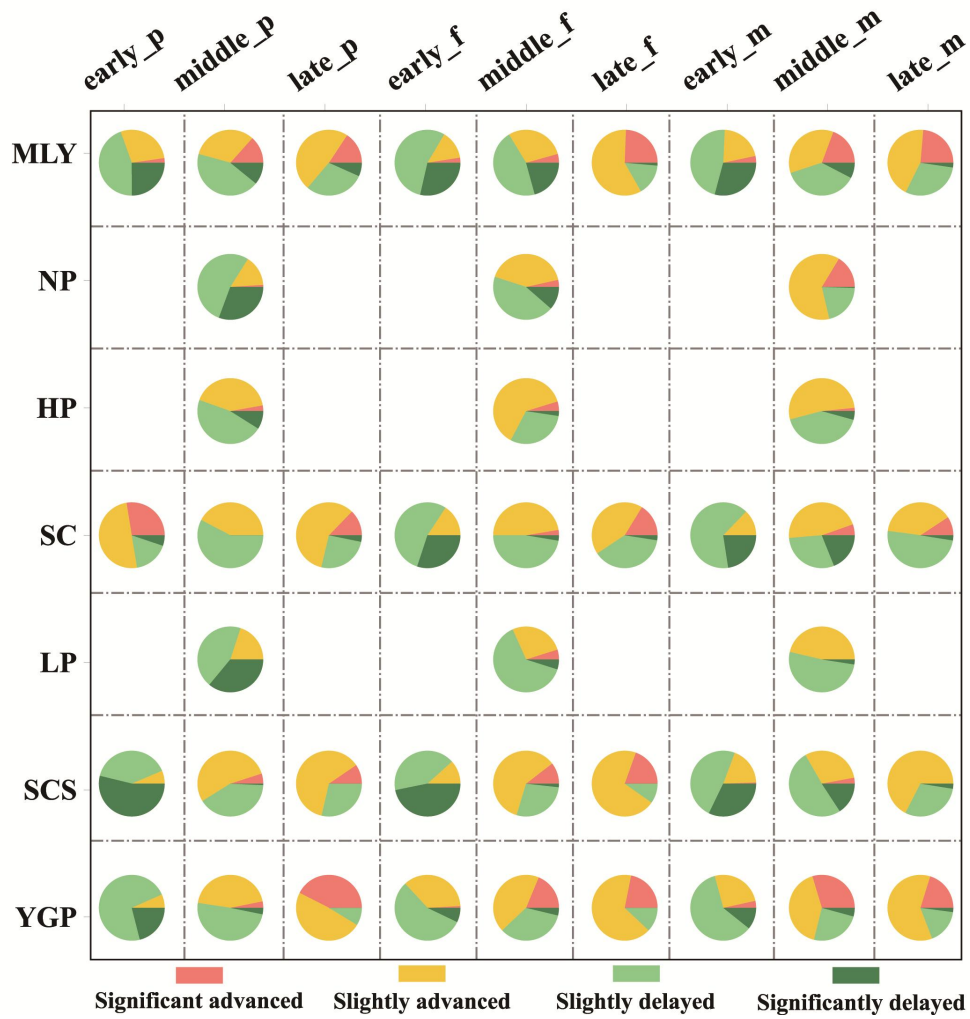
548

549

550

551

Fig. 8 Temporal trends in rice phenological dates at the county scale from 2003 to 2022 (a: early-rice transplanting dates; b: middle-rice transplanting dates; c: late-rice transplanting dates; d: early-rice heading dates; e: middle-rice heading dates; f: late-rice heading dates; g: early-rice maturity dates; h: middle-rice maturity dates; i: late-rice maturity dates)



552

553 **Fig. 9** Temporal trends in rice phenological dates at the regional level from 2003 to 2022 (early_p:
 554 early-rice transplanting dates; middle_p: middle-rice transplanting dates; late_p: late-rice
 555 transplanting dates; early_f: early-rice heading dates; middle_f: middle-rice heading dates;
 556 late_f: late-rice heading dates; early_m: early-rice maturity dates; middle_m: middle-rice
 557 maturity dates; late_m: late-rice maturity dates)

558 **Table 1 PhenoRice parameters used in the study** (EVI_{max_th}: EVI threshold above which a local
559 maxima can be considered as a peak of a growing season; EVI_{min_th}: EVI threshold below which a
560 local minima min can be considered as a start of a growing season; v11: shortest vegetative growth
561 length; v12: longest vegetative growth length; t11: shortest field growth length; t12: longest field
562 growth length; LST_{th}: minimum land surface temperature for rice planting; Winfl: time window
563 for capturing flooding signals; minndfi: threshold for NDFI; Wind_{decr}: threshold for a decline
564 window after EVI maximum; dec_{th}: percent decrease of EVI after EVI maximum)

Province	EVI _{max_th}	EVI _{min_th}	v11 (days)	v12 (days)	t11 (days)	t12 (days)	LST _{th} (°C)	Winfl (days)	minndfi	Wind _{decr} (days)	Dec _{th}
Anhui	0.4	0.25	32	72	64	120	15	24	0	64	0.5
Chongqing	0.4	0.25	64	88	96	136	15	24	0	64	0.5
Fujian	0.4	0.25	24	88	56	128	15	24	0	64	0.5
Guangdong	0.4	0.25	40	96	72	120	15	24	0	64	0.5
Guangxi	0.4	0.25	40	88	72	120	15	24	0	64	0.5
Guizhou	0.4	0.25	56	96	80	152	15	24	0	64	0.5
Hainan	0.4	0.25	56	112	80	128	15	24	0	64	0.5
Hebei	0.4	0.25	56	112	104	152	15	24	0	64	0.5
Heilongjiang	0.4	0.25	56	96	104	136	15	24	0	64	0.5
Henan	0.4	0.25	56	88	96	120	15	24	0	64	0.5
Hubei	0.4	0.25	24	112	56	152	15	24	0	64	0.5
Hunan	0.4	0.25	32	96	56	136	15	24	0	64	0.5
Jiangsu	0.4	0.25	56	88	104	136	15	24	0	64	0.5
Jiangxi	0.4	0.25	32	80	64	120	15	24	0	64	0.5
Jilin	0.4	0.25	56	96	96	136	15	24	0	64	0.5
Liaoning	0.4	0.25	56	96	104	152	15	24	0	64	0.5
Ningxia	0.4	0.25	64	88	112	152	15	24	0	64	0.5
Shaanxi	0.4	0.25	64	88	104	128	15	24	0	64	0.5
Shandong	0.4	0.25	56	80	96	120	15	24	0	64	0.5
Shanxi	0.4	0.25	64	88	104	128	15	24	0	64	0.5
Sichuan	0.4	0.25	56	96	80	160	15	24	0	64	0.5
Yunnan	0.4	0.25	24	112	56	160	15	24	0	64	0.5
Zhejiang	0.4	0.25	32	72	64	128	15	24	0	64	0.5

Table 2 Classification criteria for early, middle, and late rice by province in China

Province	Early rice		Middle rice		Late rice	
	Transplanting dates	Maturity dates	Transplanting dates	Maturity dates	Transplanting dates	Maturity dates
Anhui	110~150	190~220	130~180	240~280	190~230	270~320
Chongqing	--	--	110~160	210~280	--	--
Fujian	90~140	180~230	140~170	240~270	180~240	270~330
Guangdong	70~140	170~220	--	--	200~240	280~340
Guangxi	80~130	180~230	140~180	250~290	180~240	280~340
Guizhou	--	--	100~180	220~310	--	--
Hainan	10~80	110~190	140~180	240~280	180~220	280~320
Hebei	--	--	120~190	260~300	--	--
Heilongjiang	--	--	120~170	240~290	--	--
Henan	--	--	130~170	240~270	--	--
Hubei	110~160	170~220	110~180	230~280	180~220	270~330
Hunan	100~140	180~230	130~170	230~280	180~230	260~320
Jiangsu	--	--	150~190	260~310	--	--
Jiangxi	--	--	150~190	260~310	--	--
Jilin	90~140	180~220	130~180	230~290	180~220	270~320
Liaoning	--	--	130~170	240~280	--	--
Ningxia	--	--	130~170	260~290	--	--
Shaanxi	--	--	120~160	250~290	--	--
Shandong	--	--	130~160	250~280	--	--
Shanxi	--	--	170~200	270~300	--	--
Sichuan	--	--	140~170	250~280	--	--
Yunnan	--	--	100~170	210~300	--	--
Zhejiang	10~90	130~180	90~170	210~310	170~230	260~330